

BreathTrack: Tracking Indoor Human Breath Status via Commodity WiFi

Dongheng Zhang, Yang Hu, Yan Chen*, Senior Member, IEEE and Bing Zeng, Fellow, IEEE

Abstract—In this paper, we propose a contact-free breath tracking system, BreathTrack, to track the status of breath using the off-the-shelf WiFi devices. BreathTrack exploits the phase variation of the Channel State Information (CSI) to track human breath. To resolve the phase distortions introduced by the hardware imperfection of the commodity WiFi chips, BreathTrack utilizes both the hardware and software correction methods. The time-invariant PLL Phase Offset (PPO) is calibrated by the hardware correction using cables and splitters, while the time-varying Carrier Frequency Offset (CFO), Sampling Frequency Offset (SFO) and Packet Detection Delay (PDD) are removed by the software corrections using the phase difference between the CSI at the receiver antennas and that at the reference antenna connected from the transmitter. Moreover, BreathTrack utilizes the sparse recovery method to find the dominant path in the multipath indoor environment and derive the corresponding complex attenuation coefficient. Then, the phase variation of the complex attenuation coefficient is utilized to extract the detailed breath status and the breath rate. Extensive experiments are conducted to show that BreathTrack could estimate the breath rate with the median accuracy of over 99% in most scenarios, and could track the detailed status of breath directly using the raw phase variation.

Index Terms—Breath tracking, sparse recovery, phase distortion, commodity WiFi, vital sign.

I. INTRODUCTION

Breath rate is an important vital sign for health monitoring and medical diagnosis. While we have witnessed, in the past few years with the development of Internet of Things (IoT), the increasing research interests and progresses in ubiquitous health monitoring [1]–[4], traditional methods are intrusive that require the physical contact between human and sensors [5] [6], which affects the normal breath of human and cannot be applied to the long-term breath monitoring.

To resolve this challenge, radio frequency based monitoring schemes that can provide non-intrusive human sensing have been proposed [7]–[25], e.g., the vital-radio uses the frequency modulated continuous wave signal to estimate the breath and heart rate [7]. However, such a system is not only expensive, but also occupies a large wireless band, which limits its

Copyright (c) 2012 IEEE. Personal use of this material is permitted. However, permission to use this material for any other purposes must be obtained from the IEEE by sending a request to pubs-permissions@ieee.org.

*Corresponding author: Yan Chen (eecyan@uestc.edu.cn).

This work was partly supported by the National Natural Science Foundation of China under Grant 61672137 and 61602090, the 111 Project No. B17008, and the Thousand Youth Talents Program of China (to Yan Chen).

The authors are with the Center for Intelligent Networking and Communications (CINC), and the School of Information and Communication Engineering, University of Electronic Science and Technology of China, Chengdu, Sichuan, China, 611731. Emails: eedhzhang@std.uestc.edu.cn, {yanghu,eecyan,eezeng}@uestc.edu.cn

application. To reduce the cost, the WiFi-based methods have been proposed [8]–[12], [18]. In [8], the UbiBreathe system has been proposed to utilize the Received Signal Strength (RSS) to monitor the breath signal. Since the RSS is not very sensitive to the minor displacements in the environment, it requires users to hold the WiFi devices close to their chests to achieve reasonable performance. The amplitude of Channel State Information (CSI) has also been utilized to estimate the breath rate [9]. However, similar to the RSS, the amplitude of CSI is also not very sensitive to the minor displacement in the environment, due to which the estimation performance is limited. To achieve reasonable performance, sophisticated subcarrier selection, denoising and filtering procedures are needed. Since the frequency of breath varies in a very narrow band, i.e., about 0.2Hz, it is difficult to determine whether the estimated frequency is corresponding to the breath frequency.

Compared with the RSS and the amplitude of CSI, the phase of CSI is much more sensitive to the minor displacement in the environment, i.e., the phase of CSI is more suitable for breath rate estimation. However, the hardware imperfection of the commodity WiFi chips will introduce different kinds of phase distortions, which makes it difficult to obtain accurate CSI phase information. It has been found that the phases of the measured CSIs across packets are not correlated even in very short time intervals [26]. Therefore, it is very difficult to estimate the breath rate directly from the phase variation of the measured CSI. To solve the phase distortion problem, the PhaseBeat system was proposed in [10], which utilizes the phase difference between receiver antennas to eliminate the phase distortion. However, since the CSI measured on the antennas is affected by the minor displacement caused by breath, the phase difference between antennas is actually the subtraction of two periodic signals, which makes the model in [10] inaccurate.

Another challenge for the breath tracking in the indoor environment is the multipath effect. In a multipath indoor environment, the received signal is not periodic due to the aggregation of the multipath effect, and thus the breath rate cannot be directly obtained from the frequency components of the CSI. Moreover, the breath may be interrupted due to various factors such as talking, thinking or even some unconscious behaviors. In such a case, only the estimation of the breath rate may not be enough. Instead, it would be more significant if we could track the detailed breath status, i.e., the time domain breath waveform similar to the Electrocardiography (ECG) signals. Such detailed breath status could be an important indicator for disease diagnosis. However, the performance of the existing WiFi-based solutions is quite limited when utilized

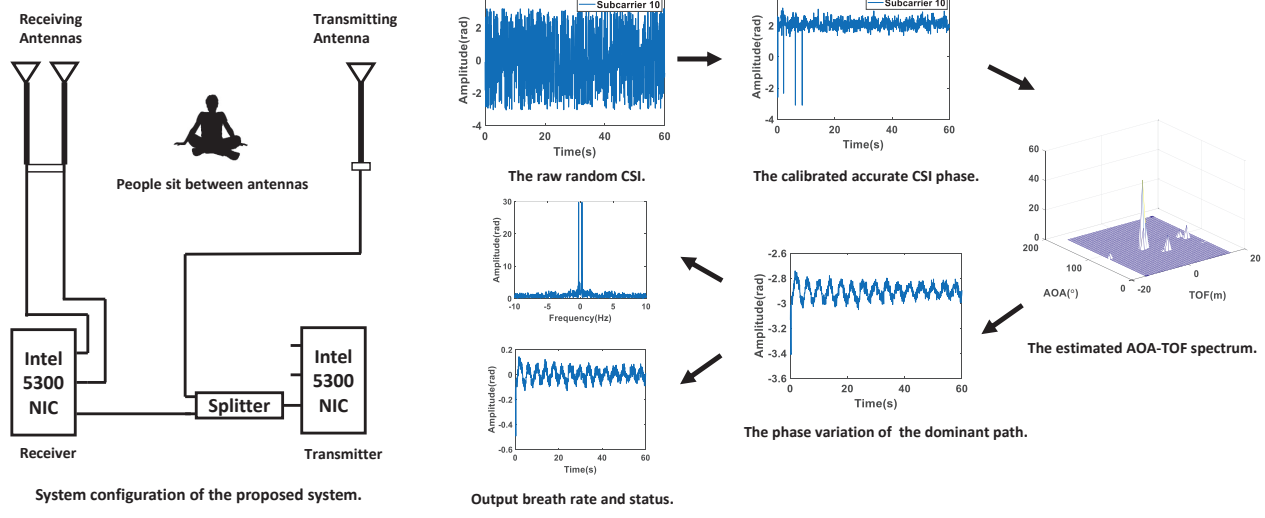


Fig. 1: An illustration of the BreathTrack system. The raw CSI is calibrated according to the signal of the reference antenna which is connected from the transmitter. Then, the AOA-TOF of received signal is jointly estimated with the sparse recovery method. After that, the phase variation of the dominant path is extracted. Finally, the breath rate and the breath status are output.

to track the detailed breath status.

To resolve the challenges, in this paper, we propose a contact-free breath tracking system using the off-the-shelf WiFi devices, BreathTrack, to track the human breath. BreathTrack exploits the phase variation of the CSI to track human breath. To avoid the phase distortions and obtain the accurate phase information, BreathTrack combines the hardware and software corrections. Specifically, the time-invariant PPL Phase Offset (PPO) is calibrated by the hardware correction using cables and splitters, while the time-varying Carrier Frequency Offset (CFO), Sampling Frequency Offset (SFO) and Packet Detection Delay (PDD) are removed by the software corrections using the phase difference between the CSI at the receiver antennas and that at the reference antenna connected from the transmitter antenna. To eliminate the multipath effect in the indoor environment, BreathTrack utilizes the sparse recovery method to find the dominant path in the environment and obtain the corresponding complex attenuation coefficient of this dominant path from the CSI. Then, the phase variation of the complex attenuation coefficient is utilized to extract the detailed breath status and the breath rate. Extensive experiments are conducted to show that BreathTrack could estimate the breath rate with the median accuracy of over 99% in most scenarios. Besides the breath rate, BreathTrack could track the detailed status of breath directly using the raw phase variation.

The contributions of BreathTrack are as follows

- BreathTrack is the first system that can track the detailed status of breath using the off-the-shelf WiFi devices.
- BreathTrack proposes hardware and software correction methods to remove both the time-invariant and time-varying phase distortions and thus obtain accurate CSI.
- BreathTrack proposes a joint AOA-TOF sparse recovery method to eliminate the multipath effect in the indoor environment and extract the information of the dominant path to track the status of breath.

The rest of the paper is organized as follows. Section II presents the system model and the sparse recovery theory of the joint AOA-TOF estimation, and Section III analyzes the performance of the joint AOA-TOF estimation. In Section IV, we illustrate in detail how to obtain accurate CSI phase and track the status of breath. The extensive experimental results are shown in Section V. Finally, conclusions are drawn in Section VI.

II. THEORETICAL MODEL

In this section, we first present the CSI model of breath estimation and the challenges. Then, we introduce the CSI model of array signal processing. Finally, we illustrate how to extract the CSI phase variation caused by breath. The system model of BreathTrack is shown in Fig. 1.

A. CSI Model of Breath Detection

Let us first consider the ideal case without the multipath effect. In such a case, the CSI can be expressed as

$$y(t) = h_0 e^{-j2\pi \frac{\tilde{d}(t)}{\lambda}}, \quad (1)$$

where $y(t)$ denotes the CSI, h_0 denotes the complex attenuation of the path, λ denotes the wavelength of the signal, and $\tilde{d}(t)$ is the length of the path.

With the minor displacement caused by breath, the CSI affected by a static human can be rewritten as

$$y(t) = h_0 e^{-j2\pi \frac{d_0 + d(t)}{\lambda}}, \quad (2)$$

where d_0 is the time-invariant path length and $d(t)$ denotes the additional dynamic path length caused by breath.

From (2), we can see that in the ideal case with a single path, the breath status can be derived directly from the phase variation of $y(t)$. However, in practice, there exists several

propagation paths in typical indoor environment due to the multipath effect. In addition, the CSI would be perturbed by the noise introduced at the receiver, which is usually assumed to be additive white Gaussian noise. Thus, the CSI in the multipath environment can be expressed as

$$y(t) = \sum_{l=1}^L h_l e^{-j2\pi \frac{d_{l0}+d_l(t)}{\lambda}} + e(t), \quad (3)$$

where L denotes the number of propagation paths and $e(t)$ denotes the noise. d_{l0} is the time-invariant length of l th path and $d_l(t)$ denotes the additional dynamic path length caused by breath.

According to (3), the CSI characterizes the multipath propagation environment. In such a case, without separating the signal affected by the human breath from the multipath signals, one may only estimate the frequency of breath signal using spectral analysis techniques rather than the whole time domain shape of the breath signal. Although pioneer works have tried to extract the time domain breath signal using subcarrier selection, denoising and filtering, the sophisticated procedures degrade the reliability, especially when the breath status changes quickly [9]. Moreover, the phase of the measured CSI from the commodity WiFi chips is generally distorted due to the imperfect internal circuit, which makes it very difficult to estimate the breath status from the phase variation of the measured CSI [26]. To resolve the above challenges, we propose to use the array signal processing techniques to address the multipath effect and adopt both the hardware and software correction methods to obtain accurate CSI from the commodity WiFi chip, which will be introduced in detail later.

B. CSI Model of Array Signal Processing

Array signal processing techniques, which focus on using organized sensors to detect signal and extract the information in need, has been well developed in the past decades [27]. Since modern WiFi devices are usually equipped with several antennas, researchers have utilized the array signal processing techniques to extract information from the WiFi devices, e.g., the estimation of Angle of Arrival (AOA) information [28], [29]. As one of the most well-known algorithm, Multiple Signal Classification (MUSIC) algorithm generates the signal subspaces and noise subspaces from the eigenvalue decomposition on the autocorrelation matrix, and then obtains the AOA estimation via orthogonality between the signal subspaces and the steering matrix. However, there are several limitations of the MUSIC algorithm, which makes it unsuitable for the off-the-shelf WiFi devices in indoor environments. Firstly, MUSIC requires that the number of antennas should be larger than the number of paths, which generally cannot be satisfied in the WiFi systems. Secondly, the performance of MUSIC will degrade rapidly if the signals from different paths are coherent, i.e., there are constant phase shifts between signals from different paths. Unfortunately, in an indoor environment, all the propagation paths from a specific transmitter are coherent because they are transmitted from the same device with the same center frequency, which degrades the performance of MUSIC. Although there are methods proposed to solve the

problems that are caused by the coherent signals [30], they all decrease the equivalent number of antennas, which limits the performance of estimation using the off-the-shelf WiFi devices.

To resolve the challenges, the algorithms based on sparse recovery have been proposed. It was shown that better resolution can be achieved [31], especially in the low SNR scenarios [32]. In the following, we will show how to use sparse recovery to jointly estimate the AOA and the time of flight (TOF).

Let θ_l and τ_l denote the AOA and TOF of the l^{th} path, respectively. Suppose that there are M antennas equipped in a uniform linear array with antennas space interval d , and K subcarriers with frequency interval Δf . Let α_l denote the complex attenuation of the signal from l^{th} path, which is assumed to be the same for all antennas and subcarriers. Thus, the relative phase between adjacent antennas and subcarriers of the l^{th} path can be expressed as

$$\Phi(\theta_l) = e^{-j2\pi d \cos \theta_l / \lambda}, \quad (4)$$

and

$$\Phi(\tau_l) = e^{-j2\pi \Delta f \tau_l}. \quad (5)$$

Therefore, the joint phase shift from the CSI of the m^{th} antenna and the k^{th} subcarrier to that of the first antenna and the first subcarrier is given by

$$\begin{aligned} \Phi_{mk}(\theta_l, \tau_l) = \exp \left(-j2\pi \left((k-1)\Delta f \tau_l + f_0 \frac{(m-1)d \cos \theta_l}{c} \right. \right. \\ \left. \left. + (k-1)\Delta f \frac{(m-1)d \cos \theta_l}{c} \right) \right), \end{aligned} \quad (6)$$

where f_0 denotes the carrier frequency of the signal.

With M antennas and K subcarriers, the phase shift vector can be written as

$$a(\theta_l, \tau_l) = [1 \ \Phi_{21}(\theta_l, \tau_l) \ \dots \ \Phi_{mk}(\theta_l, \tau_l) \ \dots \ \Phi_{MK}(\theta_l, \tau_l)]^T. \quad (7)$$

Combining all the L paths, the steering matrix is defined as

$$A = [a(\theta_1, \tau_1), a(\theta_2, \tau_2), \dots, a(\theta_L, \tau_L)]. \quad (8)$$

Thus, considering the measurement error caused by noise, the measured CSI can be expressed as

$$y = \sum_{l=1}^L a(\theta_l, \tau_l) \alpha_l + e = A\alpha + e, \quad (9)$$

where α_l denotes the complex attenuation of the signal from the l^{th} path.

To cast (9) into a sparse recovery problem, let us define a AOA-TOF grid as follows

$$\overline{\theta\tau} = [\overline{(\theta_1, \tau_1)}, \overline{(\theta_2, \tau_2)}, \dots, \overline{(\theta_N, \tau_N)}], \quad (10)$$

where N denotes the number of grid points. The overline is introduced to distinguish the grid points and actual paths.

Similar to (7), the phase shift vector of the grid can be written as

$$\overline{a(\theta_n, \tau_n)} = [1 \ \Phi_{21}(\theta_n, \tau_n) \ \dots \ \Phi_{mk}(\theta_n, \tau_n) \ \dots \ \Phi_{MK}(\theta_n, \tau_n)]^T. \quad (11)$$

According to (8) and (11), the new steering matrix which contains all the grid points can be written as

$$\bar{A} = [\overline{a(\theta_1, \tau_1)}, \overline{a(\theta_2, \tau_2)}, \dots, \overline{a(\theta_N, \tau_N)}], \quad (12)$$

Thus, the measured CSI and the complex attenuation vector can be expressed as

$$y = \bar{A}\bar{\alpha} + e, \quad (13)$$

with $\bar{\alpha}$ being the complex attenuation vector

$$\bar{\alpha} = [\alpha_1, \alpha_2, \dots, \alpha_N], \quad (14)$$

where α_n equals to the complex attenuation coefficient if there exists signal with the AOA of θ_n and TOF of τ_n , otherwise, α_n equals to zero. Thus, there are at most L non-zero elements which correspond to the L paths. Apparently, the number of grid points can be much larger than L , i.e., $L \ll N$, which means that $\bar{\alpha}$ is a sparse vector. As a result, the problem can be solved using minimum norm methods [31], and the optimization problem can be formulated as follows

$$\begin{aligned} \min \quad & \|\bar{\alpha}\|_1, \\ \text{s.t.} \quad & \|y - \bar{A}\bar{\alpha}\|_2^2 \leq \beta, \end{aligned} \quad (15)$$

where β is the parameter determined by the noise level. Once the minimal norm problem been solved, we can obtain A from \bar{A} by selecting the columns of which α_n is non-zero.

C. Breath rate estimation based on sparse estimation

In the subsection above, we have introduced the model of jointly estimating AOA-TOF based on the sparse recovery. To extract the signal variation caused by breath, a straightforward approach is to estimate the AOA-TOF of the received signal at different time slots independently and obtain the breath information from the AOA-TOF variation. However, since the displacement caused by breath is at the centimeter scale, the AOA variation resulted from the displacement is negligible while the TOF variation is also very small. To estimate the breath rate by the TOF variation directly, the grid of TOF should be intensive enough, i.e., the TOF grid needs to be set at the millimeter scale, which makes the computation complexity too high. Also, treating samples at different time slots independently does not fully utilize the correlation of data in time domain.

Since the AOA-TOF changes slowly compared with the speed of transmitting packets, we are motivated to combine the samples at different slots to obtain robust estimation. However, combining the samples at different slots directly would increase the computation cost dramatically, which makes it unapplicable to practical systems. To resolve the problem, we utilize the l_1 -SVD algorithm proposed in [31] to improve the accuracy and robustness of the AOA-TOF estimation. The l_1 -SVD algorithm [31] is a tractable approach to use a large number of time samples coherently. The idea is to decompose the data matrix into the signal and noise subspaces, and reformulate the problem with reduced dimensions into the multiple sample sparse spectrum estimation problem.

Let Y denote T consecutive time samples of $y(t)$. Taking the SVD on Y , we have

$$Y = U\Sigma V'. \quad (16)$$

Let us keep the reduced $MK \times L$ dimensional matrix $Y_{SV} = U\Sigma D_L = YV D_L$, where $D_L = [I_L 0']$, I_L is a $L \times L$ identity matrix, and 0 is a $L \times (T-L)$ matrix of zeros. Similarly, let X and E denote T consecutive samples of $\alpha(t)$ and $e(t)$, respectively, and define $X_{SV} = XVD_L$ and $E_{SV} = EVD_L$. Then, we have

$$Y_{SV} = AX_{SV} + E_{SV}. \quad (17)$$

With the SVD, the size of the problem is reduced from T blocks of data to L , where $L \ll T$. Note that the form of (17) is the same as that of (9), which means that it could be effectively solved by the minimal norm method [31]. Although the formulation of SVD uses the information about the number of paths, L , it has been observed that incorrect determination of L has no catastrophic consequences [31]. Once we obtain the estimation of AOA-TOF, the complex attenuation coefficient can be derived, which is given by

$$\alpha(t) = A^\dagger y(t), \quad (18)$$

where A^\dagger denotes the pseudo-inverse of A . Note that A is the steering matrix in (8), which is obtained in the last subsection by jointly estimating AOA-TOF and selecting the columns of \bar{A} where the corresponding complex attenuation coefficient is non-zero. The phase variation of $\alpha(t)$ corresponds to the minor displacement caused by breath directly, which can be utilized to track the breath.

III. PERFORMANCE ANALYSIS

In this section, we discuss the performance of the sparse recovery based AOA-TOF estimation. Specifically, we mainly focus on the capability of distinguishing the multipath components. We use the block coherence proposed in [34], which can be calculated directly from the dictionary, i.e., the AOA-TOF grid, to evaluate the performance of the estimation. In this paper, we set the block size in [34] as 1. Thus, the block coherence of a grid \bar{A} , which measures the similarity between its elements, is defined as

$$\mu_B = \max_{(p \neq r)} |\overline{a(\theta_p, \tau_p)}^H a(\theta_r, \tau_r)|. \quad (19)$$

To efficiently recover the signal, the block coherence needs to satisfy the following condition [34]

$$L < \frac{\mu_B^{-1} + 1}{2}, \quad (20)$$

where L denotes the number of paths.

Here we only discuss the optimal condition that the component of the grid is well selected, i.e., we only consider the coherence between different paths and explore the fact that under which condition different paths can be separated. We first consider the case that there are two paths in the environment. In such a case, the coherence between two paths is given by

$$\mu_B = a(\theta_1, \tau_1)^H a(\theta_2, \tau_2). \quad (21)$$

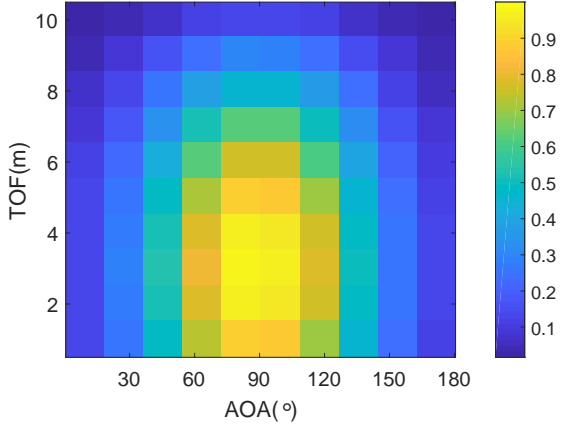


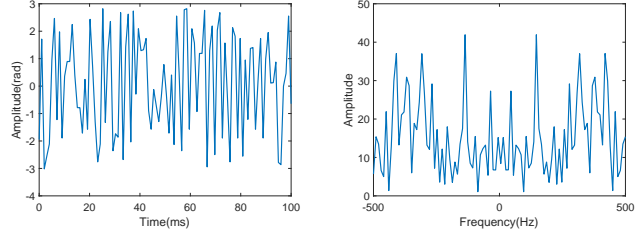
Fig. 2: The distribution of μ_B under different AOA-TOF conditions.

From (7) and (20), we can see that if two paths are well separated in space, i.e., the difference of their corresponding AOA and TOF is large, then the block coherence condition could be well satisfied. By assuming that the AOA-TOF of one path is known, we can find out under what condition the AOA-TOF of the second path can be estimated with performance guarantee. When $L = 2$, it can be derived from (24) that if $\mu_B < 1/3$, the AOA-TOF of two paths could be accurately estimated.

Although there are three antennas on the Intel 5300 NIC, we can only use two of them as one is used for correcting the distorted CSI, which will be discussed in detail in the next section. Therefore, we consider the two-antenna scenario with space interval of 2.6cm. We fix the AOA-TOF of one path as 90° and 2m, i.e., $\theta_1 = 90$ and $\tau_1 = 2/3 \times 10^8$. Then, we vary the AOA-TOF of the second path to compute the coherence defined in (20). The results are shown in Fig. 2. The AOA-TOF of the two paths could be estimated if the second path is under the blue area which satisfies the condition $\mu_B < 1/3$. Note that it generally requires the two paths are separated by 60° in AOA or 8m in TOF. Since the space of the indoor environment is quite limited, the paths in the indoor environment usually cannot satisfy such conditions, which results in estimation bias. Moreover, there are usually more than two paths in the environment, which makes the situation even worse. Fortunately, the block coherence is just a sufficient condition rather than a necessary condition. Although the coherence condition may not be satisfied in the indoor environment, if there is a dominant path, e.g., a strong light of sight (LOS) path, the AOA-TOF of the dominant path could be accurately estimated which is mainly because the coherence condition is always satisfied if there is only one path. Note that by combining the AOA and TOF estimation, the performance is improved since the joint estimation could fully utilize the resolution in both AOA and TOF dimensions.

IV. DATA PROCESSING

In this section, we will introduce in detail the data processing steps of the proposed system. Specifically, we first



(a) The raw CSI phase in time domain.
(b) The raw CSI phase in frequency domain.

Fig. 3: The raw CSI phase within 100ms.

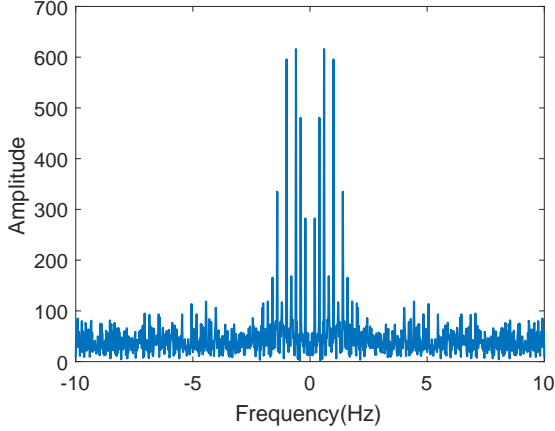


Fig. 4: The spectrum of the phase difference between antennas, which leads to wrong breath rate estimation

introduce how to obtain accurate CSI. Then, we present how to extract the phase corresponding to the breath and how to estimate the breath rate.

A. Obtaining accurate CSI for breath detection

Due to the hardware imperfection of commodity WiFi chips, the measured CSI is generally distorted by the internal circuit. Moreover, some distortions even change rapidly with time, which makes it difficult to obtain the accurate CSI measurement. Existing work has found that the phases of measured CSIs across packets are not correlated [26], which limits the application of phase variation based wireless sensing. As shown in Fig. 3, the phase of measured CSI in 0.1 second varies rapidly, which makes it impossible to extract breath rate directly.

The method in [10] proposed to utilize the phase difference between antennas to eliminate phase distortions introduced in the internal circuit. However, this method is not accurate enough because the phase of measured CSI on all antennas are affected by the minor displacement caused by breath. Thus, the phase difference between antennas is actually the subtraction of two periodic signals, which makes the method in [10] inaccurate. To validate this, we conduct simulations as follows. We assume a signal propagation path with length 2m, the path length is affected by human breath, which changes periodically with the frequency of 0.2Hz. The phase differences between

antennas are shown in Fig. 4. We can see that the peak of frequency does not correspond to the breath rate, i.e., the method based on the phase differences between antennas in [10] is inaccurate.

Before discussing how to obtain accurate CSI, we first introduce the possible distortions that will affect the phase of measured CSI. According to [38], there are mainly four kinds of phase distortions,

- Carrier Frequency Offset (CFO): Due to the hardware limitation, the central frequencies of the transmitter and the receiver are not perfectly synchronized. Although the CFO has been compensated by a CFO corrector, the residual CFO caused by the imperfect correction still distorts the CSI estimation significantly.
- Sampling Frequency Offset (SFO): The actual sampling frequency of the receiver is not consistent with its ideal value, which introduces the SFO in the estimated CSI.
- Packet Detection Delay (PDD): Packet detection delay occurs in the digital signal processing part of the received signal, which results in a time shift of the received signal.
- PLL Phase Offset (PPO): Although the antennas of the receiver share a phase-locked loop, the initial phase of signals generated by the PLL to the RF chains are different.

Although IQ imbalance also causes phase distortion, since it is negligible compared with aforementioned ones and require frequency hopping for calibration, it is out of the scope of this paper. In the ideal case, the CSI measured on the m^{th} antenna and the k^{th} subcarrier can be expressed as

$$y_{m,k}(t) = \sum_{i=1}^L \alpha_i e^{-j2\pi f_k \tau_i^m}, \quad (22)$$

where L denotes the number of paths.

With the four kinds of phase distortion mentioned above, the actual measured CSI can be expressed as

$$\begin{aligned} y_{m,k}(t) &= e^{-j2\pi(f_{CFO}t+k\Delta f(\tau_{SFO}(t)+\tau_{PDD}(t)))} \\ &\quad e^{j\varphi_{PLL_m}} \sum_{i=1}^L \alpha_i e^{-j2\pi f_k \tau_i^m}, \end{aligned} \quad (23)$$

where τ_{PDD} and τ_{SFO} denote the time shift introduced by PDD and SFO, respectively, f_{CFO} denotes the residual CFO, and φ_{PLL} denotes the time-invariant PPO.

The correction of the PPO has been well investigated in [28] and [29]. The auto-calibration algorithm in [29] can calibrate the PPO automatically, however, it requires several transmitters with known locations and the performance of calibration is limited. Since the calibration is only invoked when the receiver sets the channel, to guarantee the robustness of the phase correction, we use the method proposed in [28] which utilizes cables and splitters to correct the PPO between antennas.

While the PPO is a constant offset which can be corrected through cables and splitters, other phase distortions (CFO, SFO and PDD) are difficult to correct since they are time-variant. To the best of our knowledge, there is no existing reliable correction approach up to now. The most recent approach in [39] utilized two propagation paths to get rid of

the phase distortion. However, such a method is not reliable since it is very difficult to detect two paths stably in the indoor multipath environment using the off-the-shelf WiFi devices. Fortunately, we have found that the CFO, SFO and PDD are the same among different antennas, which makes the phase difference between antennas time-invariant in the static environment [10]. To create an artificially static environment, we connect the transmitter and receiver by a coaxial cable. By assuming that the antenna 1 at the receiver is connected with the transmitter, the measured CSI on the antenna 1 at the receiver can be expressed as

$$y_{1,k}(t) = e^{-j2\pi(f_{CFO}t+k\Delta f(\tau_{SFO}(t)+\tau_{PDD}(t)))} e^{j\varphi_{PLL_1}} \alpha_0 e^{-j2\pi f_k \tau_0}, \quad (24)$$

where α_0 and τ_0 denote the complex attenuation of the coaxial cable and the TOF in the cable, respectively.

Since the signal propagates in the coaxial cable, under the ideal case, the CSI measured on this antenna should be time-invariant. Thus, the variation of the measured CSI is only caused by the distortions, i.e., the CFO, SFO and PDD. With such information on this antenna, to eliminate the phase distortion on other antennas, the measured CSI of m^{th} antenna is multiplied with the complex conjugate of the CSI on the antenna 1 as follows

$$\begin{aligned} \hat{y}_{m,k} &= (y_{1,k})^* \times y_{m,k} \\ &= \alpha_0 e^{j2\pi f_k \tau_0} \sum_{i=1}^L \alpha_i e^{-j2\pi f_k \tau_i^m}, \end{aligned} \quad (25)$$

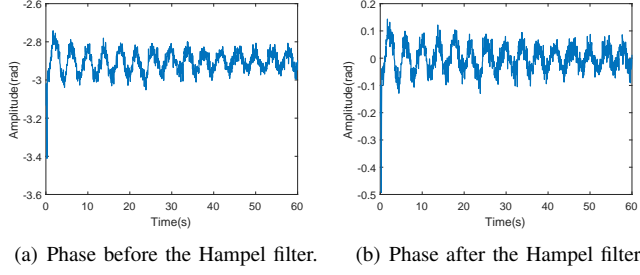
where $*$ denotes the operation of complex conjugate. Note that since φ_{PLL} can be removed as illustrated above, we omit it in (24).

By comparing (25) and (22), we can see that the modified CSI $\hat{y}_{m,k}$ is the ideal CSI $y_{m,k}$ multiplied with a constant complex coefficient. Since τ_0 is known which is determined by the length of coaxial cable, the complex coefficient will not affect the estimation of AOA-TOF and thus not affect the estimation of the breath.

B. Phase Extraction and Breath Rate Estimation

With the modified CSI $\hat{y}_{m,k}$ in (25), we utilize the sparse recovery algorithm in Section III to estimate the AOA-TOF of the paths in the environment. According to the performance analysis, with two antennas, only the AOA-TOF estimation of the dominant path is reliable. Thus, we only pick the path with the maximum amplitude in the estimated AOA-TOF spectrum to build matrix A in (8). Then, the complex coefficient of this dominant path is obtained, and the phase of this complex coefficient is extracted for breath rate estimation.

In Fig. 5 (a), we show the phase of the complex coefficient extracted via the sparse recovery. We can see that the raw phase data has very high correlation with the human breath without any further processing. Therefore, the breath rate estimation does not require sophisticated denoising, filtering and/or approximating processing steps as in the previous works [8]–[10]. Since the DC component of the phase variation is large, which may affect the breath rate estimation, we utilize



(a) Phase before the Hampel filter. (b) Phase after the Hampel filter.

Fig. 5: The phase extracted by the proposed system.

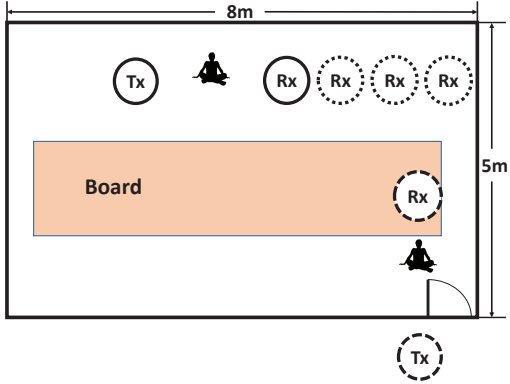


Fig. 6: The layout of the meeting room.

the Hampel Filter to remove it [10]. The window size is set as 100 samples and the threshold is set to be 0.01. As shown in Fig. 5 (b), the DC component of phase variation is perfectly removed. To further suppress the low frequency noise, we use a FIR highpass filter with the cutoff frequency 0.05Hz, which is determined by the lowest breath frequency of human. Then, we simply pick the peak of FFT spectrum of the filtered phase data as the estimation of breath rate.

V. EXPERIMENTS RESULTS

In this section, we conduct extensive real experiments to evaluate the performance of the proposed system. Specifically, we first illustrate the performance of the AOA estimation in the proposed system. Then, we show the advantages of the proposed system by comparing the raw phase data obtained in the proposed system with those obtained using existing methods which use signal variation on subcarriers to estimate breath rate [8]–[10]. Finally, we show the performance of the proposed system under different experimental settings.

We use two desktop computers equipped with the Intel 5300 NIC as the transmitter and the receiver. The Linux 802.11n CSI Tool [37] is installed on the Ubuntu desktop 14.04 LTS OS for both the transmitter and the receiver. We randomly choose channel 62, i.e., 5.31GHz center frequency with the 40MHz bandwidth, as our experimental band. The receiver operates in the “monitor” mode. It is equipped with a uniform linear array which is composed of three omnidirectional antennas, while we only use two of them since one of the port is connected with the transmitter directly. The space interval of the antennas

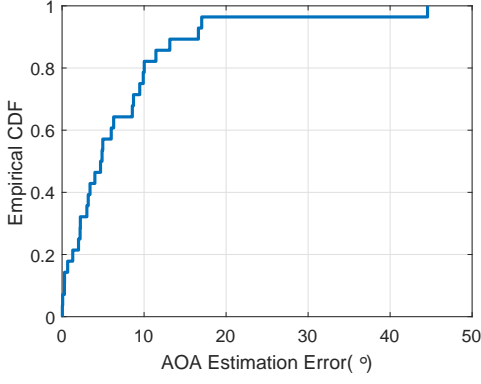


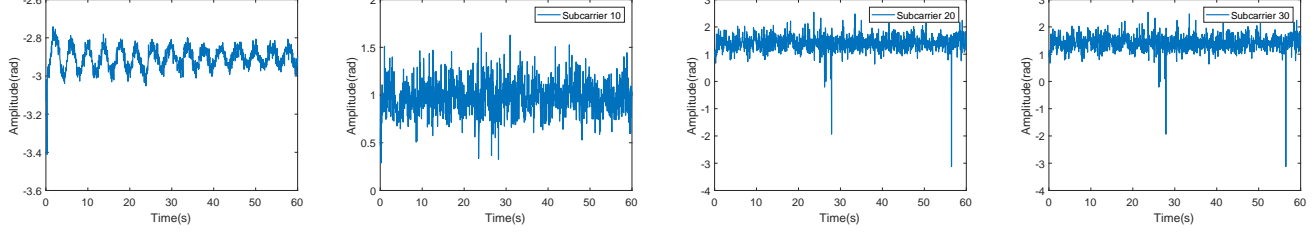
Fig. 7: The performance of the AOA estimation.

is 2.6cm, which is about the half wavelength. The transmitter operates in the “inject” mode using one omnidirectional antenna. It injects 20 packets per second. The transmitted signal is first divided into two parts using a microwave power splitter: one is fed into the transmit antenna and the other is fed into an attenuator which is connected with the receiver via a coaxial cable. The AOA-TOF estimation problem with the sparse recovery formulation is solved using the CVX tool [36]. The AOA grid spans $[1^\circ, 180^\circ]$ with $N_\theta = 90$ and the TOF grid spans $[-15m, 15m]$ with $N_\tau = 31$.

A total of 8 different participants were invited. The performance of the system is evaluated by comparing the estimated breath rate with the ground truth. To obtain the ground truths, participants are asked to synchronize their breaths with the metronome on their cellphones. Besides the controlled breath, participants are also asked to breath naturally and count their breaths manually. Experiments are conducted in a $5m \times 8m$ meeting room. The layout of the meeting room is shown in Fig. 6, where Tx and Rx denote the transmitter and receiver antennas, respectively. To test the impact of the distance between transmitter and receiver, we fix the position of transmitter antenna and vary the location of the receiver antennas. In the NLOS scenario, the transmitter antenna is deployed about 50cm outside the door. Note that the meeting room is crowded of chairs, computers and other devices, which are not shown in Fig. 6. To guarantee that the dominant path is affected by human breath, the participant sits between the transmitter and the receiver in all experiments.

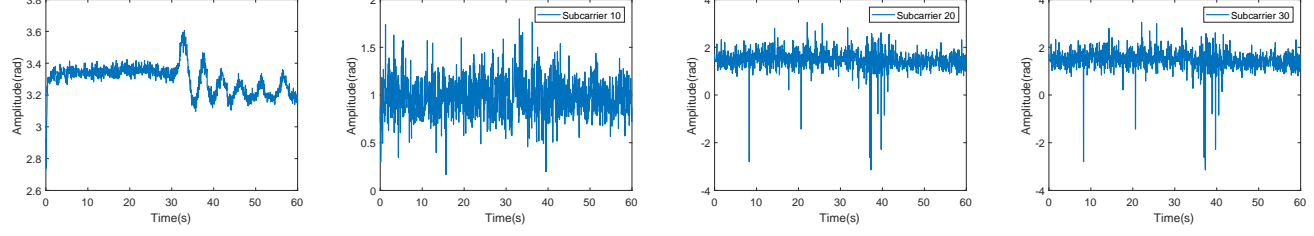
A. Performance of AOA estimation

In the first experiment, we show the performance of the AOA estimation. The transmitter is about 3m away from the receiver and the ground truth AOA varies from 60° to 120° . The empirical CDF is shown in Fig. 7, which is consistent with the performance evaluation in [32]. From Fig. 7, we can see that the estimation error of the AOA is smaller than 20° , and such an estimation bias does not affect the extraction of the phase variation significantly as we found through both simulation and experiments.



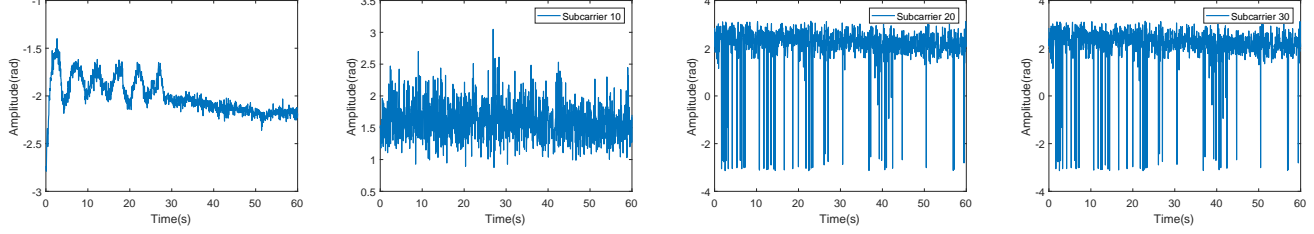
(a) Raw phase extracted from the dominant path.
 (b) Raw phase of the CSI on subcarrier 10.
 (c) Raw phase of the CSI on subcarrier 20.
 (d) Raw phase of the CSI on subcarrier 30.

Fig. 9: The case when one person breaths 15 times per minute.



(a) Raw phase extracted from the dominant path.
 (b) Raw phase of the CSI on subcarrier 10.
 (c) Raw phase of the CSI on subcarrier 20.
 (d) Raw phase of the CSI on subcarrier 30.

Fig. 10: The case when one person holds the breath first and then breath normally.



(a) Raw phase extracted from the dominant path.
 (b) Raw phase of the CSI on subcarrier 10.
 (c) Raw phase of the CSI on subcarrier 20.
 (d) Raw phase of the CSI on subcarrier 30.

Fig. 11: The case when one person breaths normally first and then holds the breath.

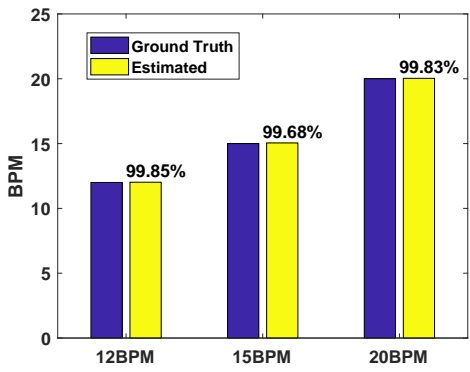


Fig. 8: Median error of breath rate estimation under different breath frequencies.

B. Performance of breath rate estimation

We first consider the LOS scenario with a single person, i.e., there is a LOS path between the transmitter and the

receiver while only one person exists in the environment. The transmitter and the receiver are separated 2m away. The participant sits in the midpoints of the transmitter and the receiver. To show the robustness of the proposed system, they are asked to breath with the frequency of 0.2Hz, 0.25Hz and 0.33Hz in different experiments, respectively. The median accuracy of the breath rate estimation of three frequencies is shown in Fig. 8. We can see that the proposed method can achieve very accurate breath rate estimation, above 99.5%, in this scenario.

Since most existing methods seem to have reasonable performance in estimating the breath rate under simple settings, to show the advantages of the propose system, we compare the raw phase variation data of different subcarriers and the raw phase extracted by the proposed system. We first ask the participant to breath with 15 BPM and the results are shown in Fig. 9. It can be seen clearly from the Fig. 9 (a) that there are 15 periods. On the contrary, although the phase of the subcarriers do show some periodicity, it is difficult to

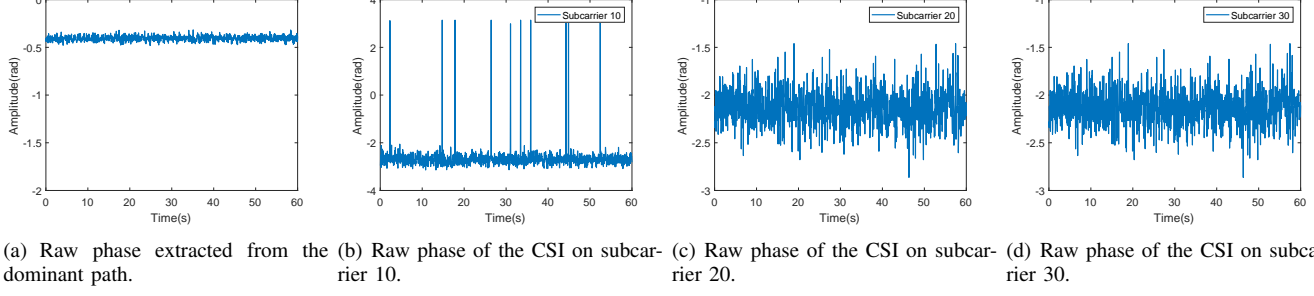


Fig. 12: The case when no person exists in the environment.

recognize the breath period based on the phase variation on the subcarriers as shown in Fig. 9 (b), (c), and (d). Note that we do check the phase variation of all different subcarriers, however, none of them could be used to judge the breath period. In all experiments of the proposed system, the raw phase data is directly related to the breath and the frequency of the breath can be easily estimated in the way similar to Fig. 9 (a) if there is no other specific illustration.

To further illustrate the advantages of proposed system, we show two more experiments in Fig. 10 and Fig. 11. Since the status of human breath may change rapidly due to many factors, such as speaking, moving or even some unconscious behaviors, it will be much more significant if one could identify the whole breath status rather than just estimate the rate. In Fig. 10, the participant is asked to hold the breath for 30s first, then take a deep breath, and finally breath normally. In Fig. 11, the participant is asked to breath normally first, and then hold the breath. As shown in Fig. 10 (a) and Fig. 11 (a), the proposed system can perfectly capture such minor and fast change of the whole breath status. However, similar to the results in Fig. 9, we cannot judge the breath status directly from the phase variation on different subcarriers as shown in (b), (c), and (d) of Fig. 10 and Fig. 11. Note that the peaks in Fig. 11 (c) and (d) are caused by the phase wrapping in $[-2\pi, 2\pi]$. We also evaluate the case when there is no person existing in the environment and the results are shown in Fig. 12. We can see from Fig. 12 (a) that the phase variation extracted from the dominant path is very stable. However, from the phase variation of different subcarriers, it is very hard to distinguish whether the signal is affected by human breath or not. This is because with or without human breath, the time domain phase variation does not show significant difference, especially for subcarrier 20 and subcarrier 30. It seems that the signal is still affected by some periodic displacement as shown in Fig. 12 (c) and (d). According to the subcarrier selection strategy used in [9], such subcarriers will be selected as “high periodicity” ones and used to calculate breath rate, which will lead to wrong breath detection.

C. Impact of distance between transmitter and receiver

In this section, we evaluate the performance of the proposed system under different distances between the transmitter and the receiver. The participants sit in the midpoints of the transmitter and the receiver, breath with the frequency of

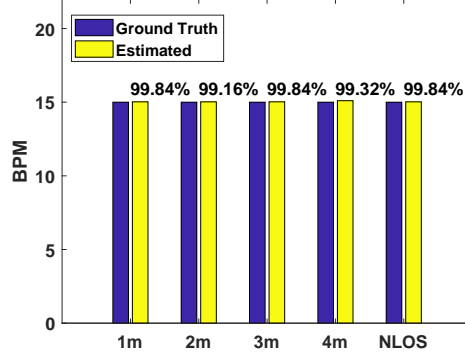


Fig. 13: Median error of breath rate estimation under different conditions of the transmitter-receiver distance and the NLOS scenario.

0.25Hz. The performance of breath rate estimation is shown in Fig. 13. As shown in the figure, the proposed system could achieve high accuracy when the distance varies from 1m to 4m. Although we do conduct the experiments under the scenario that the transmitter and the receiver are separated by 5m, the packet loss rate increases rapidly. In more than 10 experiments, the packet loss rate varies from 50% to 90%, due to which the measured CSI could not be used to estimate the breath rate. Some modifications on the CSI tool may be needed to reduce the packet loss rate to make the measured CSI useful, which however is out of the scope of this paper.

D. Impact of people's motion

Since the phase of the signal is sensitive to the minor displacements in the environment, we explore the impact of people's motion in this subsection. As shown in Fig. 14, large motions do have significant influence on the phase variation. Thus, we use a time window which is introduced in [7] with the length of 10s to remove the data affected by the large motion based on the variance. Participants sit between the transmitter and the receiver, and breath with the frequency of 0.25Hz. They are asked to chat with friends using cellphone, shake their heads, stand up and turn around in the experiments. The performance of breath rate estimation is shown in Fig. 15. As shown in the figure, using cellphone or shaking heads does not affect the breath rate estimation. Motions like standing up

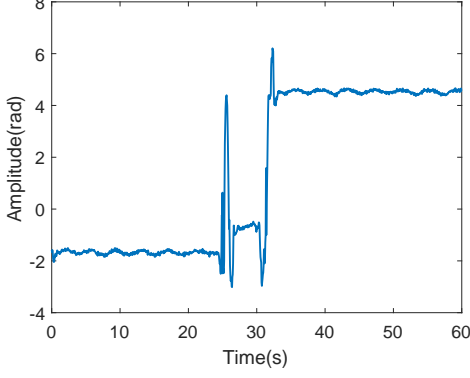


Fig. 14: The raw phase variation when the participant stands up at 24th second and sits down at 32th second.

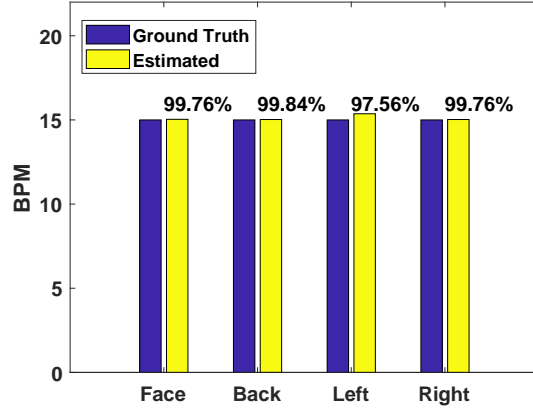


Fig. 17: Median error of breath rate estimation with different orientations of human.

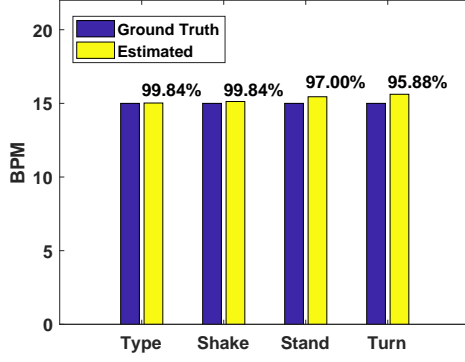


Fig. 15: Median error of breath rate estimation with the interference of motion.

or turning around does affect the performance of breath rate estimation a little bit, which is mainly because the system could only use the data that is not affected by the large motion to calculate breath rate and the motions like standing up or turning around reduce the useful data more significantly.

E. Impact of human's orientation

It has been found in previous work that the human's orientation will affect the performance of the breath estimation [9], due to the different amplitude of displacement caused by breath in different orientations. Thus, we conduct a series of experiments to evaluate the impact of human's orientation

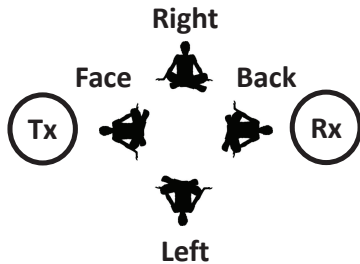


Fig. 16: The sketch of human in different orientations.

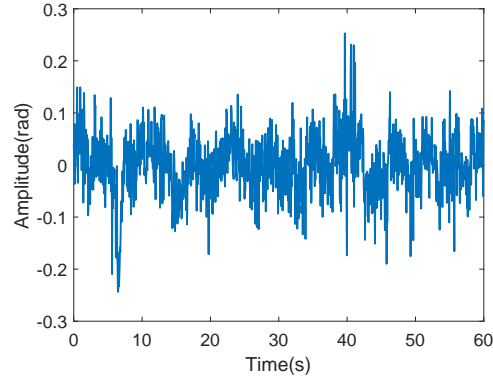
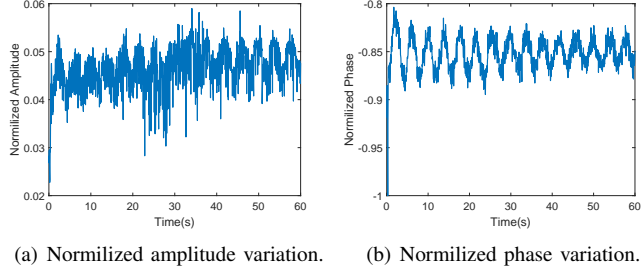


Fig. 18: Raw phase extracted from the dominant path in the NLOS scenario.

in this subsection. As shown in Fig. 16, the participant is asked to sit facing the receiver antenna, back to the receiver antenna, toward the left and right side of receiver antenna, respectively. The performance is shown in Fig. 17. We can see that benefiting from the high sensitivity of the signal phase, the orientation does not affect much the breath rate estimation of the proposed system.

F. Breath rate estimation in NLOS scenarios

For indoor localization applications, the AOA-TOF based algorithms require the LOS path to accurately locate the transmitter. In the NLOS scenarios, it cannot locate the transmitter accurately since the estimated AOA-TOF does not correspond to the location of transmitter directly. Nevertheless, since our goal is to extract the signal of the dominant path in the environment rather than locate the transmitter, the proposed system still works in the NLOS scenarios. In this experiment, the transmitter is moved outside the meeting room. The participant sits 1m from the receiver and breath with the frequency of 0.25Hz. The performance of the breath rate estimation is shown in Fig. 13. As shown in the figure, the proposed system could also work in the NLOS scenarios with high accuracy. While the breath rate estimation is not affected



(a) Normilized amplitude variation. (b) Normilized phase variation.

Fig. 19: The comparison of CSI amplitude and phase variation.

significantly in NLOS case, the raw phase variation becomes more unstable compared to the LOS scenarios, as shown in Fig. 18. This is mainly due to the extra attenuation in the NLOS scenarios.

G. Comparison of the CSI amplitude and phase

In this section, we compare the amplitude and phase variation extracted by the proposed system to demonstrate that CSI phase is more sensitive to human breath compared with the CSI amplitude. For the sake of fairness, both amplitude and phase are normalized to [0, 1]. As shown in Fig. 19, it is more difficult to recognize breath period from the amplitude variation. This is because the amplitude variation caused by human breath is too small to capture according to the radar range equation [35], which makes it suffer from random noise. In contrast, the phase variation is linear with the minor displacement caused by human breath, which makes it more sensitive and suitable for breath status tracking. We show the Cumulative Distribution Functions(CDF) of breath rate estimation error in Fig. 20. We can see that the performance with CSI phase is much better than that with CSI amplitude.

H. Impact of human locations

In previous sections, we assume that the person stays close to the link of the transmitter and receiver to make sure that the human breath would have enough impacts on the received signal. Here, we conduct experiments to evaluate the impact of the distance from the human location to the transmitter-receiver link. The person initially stays at the midpoint of the transmitter and receiver, and then moves away perpendicularly as shown in Fig. 21. The transmitter and receiver are separated by 2.2m. The breath rate estimation accuracy versus the distance between the person and the midpoint is shown in Fig. 22. The proposed system could provide very accurate breath rate estimation when the distance is within 2m and the accuracy begins degraded with a larger distance. The phase variation when person stays with a different distance is shown in Fig. 23. The phase variation becomes smaller, due to which it is more difficult to recognize breath period with a larger distance. This is mainly because the reflected signal becomes weaker and has less impact on the received signal when the person moves away.

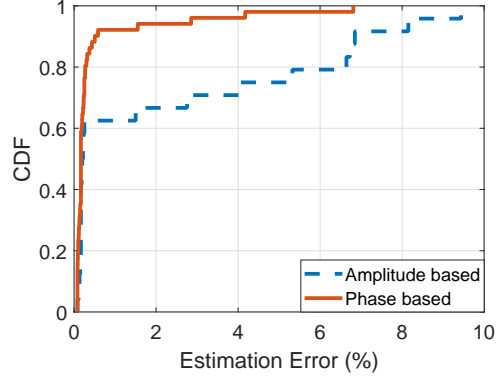


Fig. 20: Comparison of breath rate estimation accuracy

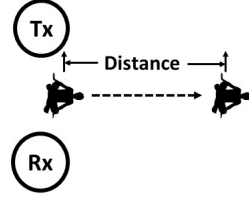


Fig. 21: The sketch of human at different locations.

I. Multi-person scenario

The proposed system can also work in the multi-person scenario under the assumption that the breath rate of different participants are different. Three participants are invited to breath with the frequency of 0.2Hz, 0.25Hz, and 0.33Hz, respectively. The performance of the breath rate estimation for the three participants are shown in Fig. 24. Due to the fact that the distances between the participants and the receiver are different, the reflected signal strengths are different, which makes the performance slightly different. The person 2 with 15BPM rate is the one closest to the receiver and thus the rate estimation is most accurate, while person 3 with 20BPM rate is the farthest one from the receiver and thus the rate estimation is least accurate.

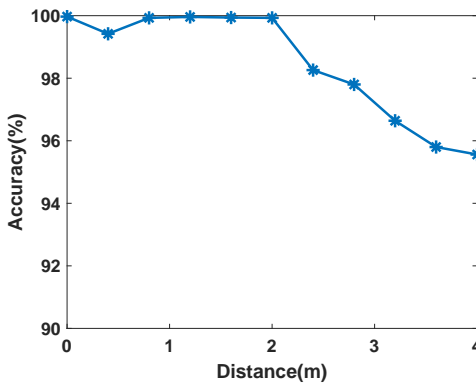


Fig. 22: Estimation accuracy versus the distance.

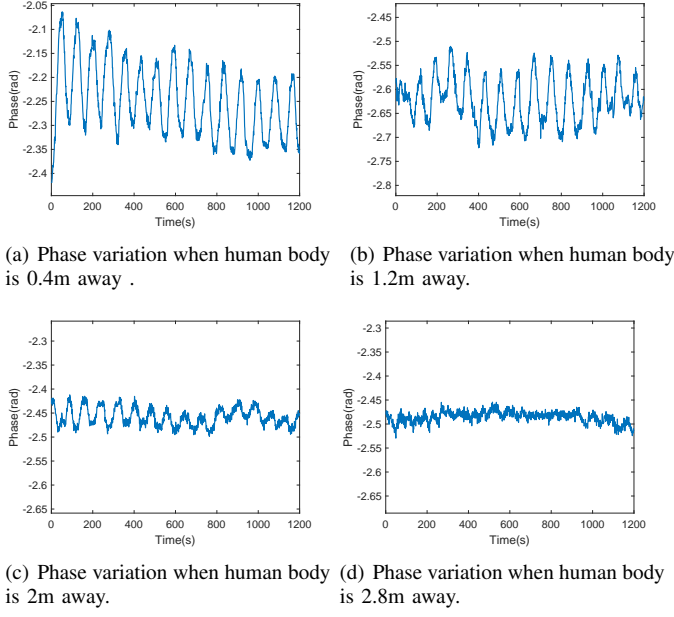


Fig. 23: Phase variation when the person stays with a different distance.

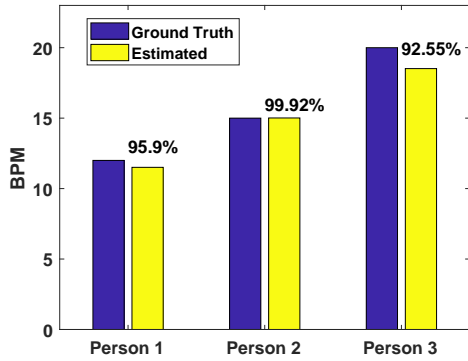


Fig. 24: Median error rate of breath rate estimation in the three persons scenario.

VI. CONCLUSION

In this paper, we proposed BreathTrack, the first system that can track the detailed status of breath using the off-the-shelf WiFi devices. To achieve this, we proposed hardware and software correction methods to remove both the time-invariant and time-varying phase distortions introduced by the hardware imperfection of the commodity WiFi chips and thus obtain the accurate CSI. We also proposed a joint AOA-TOF sparse recovery method to eliminate the multipath effect in the indoor environment and extract the information of the dominant path to track the status of breath. Experimental results show that BreathTrack can achieve high accurate breath rate estimation and track the detailed status of breath. The proposed system is also applicable in other wireless sensing applications, such as activity recognition [18], events detection [11] and speed estimation [12].

REFERENCES

- [1] M. Liu and M. Huang, "Asthma Pattern Identification via Continuous Diaphragm Motion Monitoring", *IEEE Trans. Multi-Scale Comput. Syst.*, vol. 1, no. 2, pp. 76-84, Apr. 2015.
- [2] I. Bisio, A. Delfino, A. Grattarola, F. Lavagetto and A. Sciarrone, "Ultrasounds-based Context Sensing Method and Applications over the Internet of Things", *IEEE Internet Things J.*, vol. 5, no. 5, pp. 3876-3890, Oct. 2018.
- [3] Igor Bisio, Fabio Lavagetto, Mario Marchese, Andrea Sciarrone, "A Smartphone-Centric Platform for Remote Health Monitoring of Heart Failure", *Wiley International Journal of Communication Systems*, vol. 28, no. 11, pp. 1753-1771, July 2015.
- [4] P. Verma and S. K. Sood, "Fog Assisted-IoT Enabled Patient Health Monitoring in Smart Homes," *IEEE Internet of Things Journal*, vol. 5, no. 3, pp. 1789-1796, June 2018.
- [5] iBabyGuard. <http://www.ibabyguard.com/>.
- [6] VivoSense. Sensors: Equivital. <https://www.vivosense.com/portfolio/equivital/>
- [7] F. Adib., H. Mao, Z. Kabelac., D. Katabi and R. C. Miller. "Smart homes that monitor breathing and heart rate," *ACM CHI*, 2015.
- [8] H. Abdellasser, K. A. Harras and M. Youssef, "UbiBreathe: A Ubiquitous non-Invasive WiFi-based Breathing Estimator", *ACM MobiHoc* 2015.
- [9] X. Liu, J. Cao, S. Tang, J. Wen, and P. Guo, "Contactless Respiration Monitoring Via Off-the-Shelf WiFi Devices", *IEEE Trans. Mobile Comput.*, vol. 15, no. 10, pp. 2466-2479, Oct. 2016.
- [10] X. Wang, C. Yang and S. Mao, "PhaseBeat: Exploiting CSI phase data for vital sign monitoring with commodity WiFi devices," *IEEE ICDCS*, 2017.
- [11] Q. Xu, Y. Chen, B. Wang and K. J. R. Liu, "TRIEDS: Wireless Events Detection Through the Wall", *IEEE Internet Things J.*, vol. 4, no. 3, pp. 723-735, Jun. 2017.
- [12] F. Zhang, C. Chen, B. Wang, K. J. R. Liu, "WiSpeed: A Statistical Electromagnetic Approach for Device-Free Indoor Speed Estimation", *IEEE Internet Things J.*, vol. 5, no. 3, pp. 2163-2177, Jun. 2018.
- [13] C. Chen, B.B. Wang, Y. Han, Yan Chen, F. Zhang, H.Q. Lai, and K.J.R. Liu, "TR-BREATH: Time-Reversal Breathing Rate Estimation and Detection", *IEEE Trans. on Biomedical Engineering*, vol 65, no 3, pp.489 - 501, March 2018.
- [14] Q.Y. Xu, Yan Chen, B.B. Wang, and K.J.R. Liu, "Radio Biometrics: Human Recognition Through a Wall", *IEEE Trans. on Information Forensics and Security*, vol. 12, no. 5, pp. 1141-1155, May 2017.
- [15] C. Chen, Yan Chen, Y. Han, H.Q. Lai, and K.J.R. Liu, "Achieving Centimeter Accuracy Indoor Localization on WiFi Platforms: A Frequency Hopping Approach", *IEEE Internet of Things Journal*, vol. 4, no. 1, pp. 111-121, Feb. 2017.
- [16] C. Chen, Yan Chen, Y. Han, H.Q. Lai, F. Zhang, and K.J.R. Liu, "Achieving Centimeter Accuracy Indoor Localization on WiFi Platforms: A Multi-Antenna Approach", *IEEE Internet of Things Journal*, vol. 4, no. 1, pp. 122-134, Feb. 2017.
- [17] C. Chen, Y. Han, Yan Chen, and K.J.R. Liu, "Indoor Global Positioning System with Centimeter Accuracy Using Wi-Fi", *IEEE Signal Processing Magazine*, vol 33, no 6, pp.128-134, Nov 2016.
- [18] Y. Gu, F. Ren and J. Li, "PAWS: Passive Human Activity Recognition Based on WiFi Ambient Signals", *IEEE Internet Things J.*, vol. 3, no. 5, pp. 796-805, Oct. 2016.
- [19] S. Di Domenico, M. De Sanctis, E. Cianca, F. Giuliano and G. Bianchi. "Exploring Training Options for RF Sensing Using CSI", *IEEE Commun. Mag.* , vol. 56, no. 5, pp. 116-123, May 2018.
- [20] W. Wang, Alex. X. Liu, M. Shahzad, K. Ling and S. Lu. "Device-Free Human Activity Recognition Using Commercial WiFi Devices", *IEEE J. Sel. Areas Commun.*, vol. 35, no. 5, pp. 1118-1131, May 2017.
- [21] W. Wang, Alex. X. Liu, M. Shahzad, K. Ling and S. Lu. "Understanding and Modeling of WiFi Signal Based Human Activity Recognition", *ACM Mobicom*, 2015.
- [22] Y. Wang, J. Liu, Y. Chen, M. Gruteser, J. Yang and H. Liu, "E-eyes: Device-free Location-oriented Activity Identification Using Fine-grained WiFi Signatures", *ACM Mobicom*, 2014.
- [23] C. Wu, Z. Yang, Z. Zhou, X. Liu, Y. Liu and J. Cao, "Non-Invasive Detection of Moving and Stationary Human With WiFi", *IEEE J. Sel. Areas Commun.*, vol. 33, no. 11, Nov. 2015.
- [24] W. Xi, J. Zhao, X. Li, K. Zhao, S. Tang, X. Liu and Z. Jiang, "Electronic frog eye: Counting crowd using WiFi", *IEEE INFOCOM*, 2014.
- [25] S. Di Domenico, G. Pecoraro, E. Cianca and M. De Sanctis, "Trained-once device-free crowd counting and occupancy estimation using WiFi: A Doppler spectrum based approach", *IEEE WiMob*, 2016.

- [26] R. Nandakumar, B. Kellogg, and S. Gollakota. "Wi-fi gesture recognition on existing devices," arXiv:1411.5394, 2014.
- [27] H. Krim and M. Viberg, "Two decades of array signal processing research: the parametric approach," *IEEE Signal Process. Mag.*, vol. 13, no.4, pp. 67-94, Jul. 1996.
- [28] J. Xiong and K. Jamieson, "ArrayTrack: A Fine-Grained Indoor Location System," *USENIX NSDI*, 2013.
- [29] J. Gjengset, J. Xiong, G. McPhillips, and K. Jamieson. "Phaser: enabling phased array signal processing on commodity WiFi access points," *ACM MobiCom*, 2014.
- [30] M. Kotaru, K. Joshi, D. Bharadia, and S. Katti, "Spotfi: Decimeter Level Localization Using WiFi," *ACM SIGCOMM*, 2015.
- [31] D. Malioutov, M. Cetin, and A. S. Willsky, "A sparse signal reconstruction perspective for source localization with sensor arrays," *IEEE Trans. Signal Process.*, vol. 53, no.8, Aug. 2005
- [32] W. Gong and J. Liu, "Robust indoor wireless localization using sparse recovery," *IEEE ICDCS*, 2017.
- [33] E. J. Candès and M. B. Wakin, "An introduction to compressive sampling," *IEEE Signal Processing Mag.*, vol. 25, no. 2, pp. 21-30, Mar. 2008.
- [34] Eldar Y C, Kuppinger P, Bolcskei H. "Block-sparse signals: Uncertainty relations and efficient recovery," *IEEE Trans. Signal Process.*, vol. 58, no. 6, pp. 3042-3054, June 2010
- [35] B. R. Mahafza, "*Radar systems analysis and design using MATLAB*". CRC Press, 2002.
- [36] CVX solvers, <http://cvxr.com/cvx/doc/solver.html>.
- [37] D. Halperin, W. Hu, A. Sheth, and D. Wetherall, "Tool release: gathering 802.11n traces with channel state information," *ACM SIGCOMM CCR*, 2011.
- [38] Y. Zhuo, H. Zhu, H. Xue, and S. Chang. "Perceiving Accurate CSI Phases with Commodity WiFi Devices," *IEEE INFOCOM*, 2017.
- [39] M. Kotaru and S. Katti, "Position Tracking for Virtual Reality Using Commodity WiFi," *IEEE CVPR*, 2017.



Dongheng Zhang received the B.S. degree from the School of Electronic and Engineering, University of Electronic Science and Technology of China, Chengdu, China, in 2017. He is currently pursuing the Ph.D. degree at the School of Information and Communication Engineering, University of Electronic Science and Technology of China. His research interests are in signal processing, wireless communications and networking.

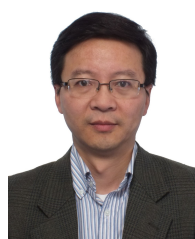


Yang Hu received the B.S. and Ph.D. degrees in electrical engineering from the University of Science and Technology of China, Hefei, China, in 2004 and 2009 respectively. She was with the University of Maryland Institute for Advanced Computer Studies as a research associate from 2010 to 2015. She is currently an associate researcher with the School of Information and Communication Engineering at the University of Electronic Science and Technology of China, Chengdu, China. Her current research interests include computer vision, machine learning and multimedia signal processing.



Yan Chen (SM'14) received the bachelor's degree from the University of Science and Technology of China in 2004, the M.Phil. degree from the Hong Kong University of Science and Technology in 2007, and the Ph.D. degree from the University of Maryland, College Park, MD, USA, in 2011. He was with Origin Wireless Inc. as a Founding Principal Technologist. Since Sept. 2015, he has been a full Professor with the School of Information and Communication Engineering at the University of Electronic Science and Technology of China. His research interests include multimedia, signal processing, game theory, and wireless communications.

He was the recipient of multiple honors and awards, including the best student paper award at the PCM in 2017, best student paper award at the IEEE ICASSP in 2016, the best paper award at the IEEE GLOBECOM in 2013, the Future Faculty Fellowship and Distinguished Dissertation Fellowship Honorable Mention from the Department of Electrical and Computer Engineering in 2010 and 2011, the Finalist of the Dean's Doctoral Research Award from the A. James Clark School of Engineering, the University of Maryland in 2011, and the Chinese Government Award for outstanding students abroad in 2010.



Bing Zeng (M'91-SM'13-F'16) received his BEng and MEng degrees in electronic engineering from University of Electronic Science and Technology of China (UESTC), Chengdu, China, in 1983 and 1986, respectively, and his PhD degree in electrical engineering from Tampere University of Technology, Tampere, Finland, in 1991.

He worked as a postdoctoral fellow at University of Toronto from September 1991 to July 1992 and as a Researcher at Concordia University from August 1992 to January 1993. He then joined the Hong Kong University of Science and Technology (HKUST). After 20 years of service at HKUST, he returned to UESTC in the summer of 2013, through Chinas 1000-Talent-Scheme. At UESTC, he leads the Institute of Image Processing to work on image and video processing, 3D and multi-view video technology, and visual big data.

During his tenure at HKUST and UESTC, he graduated more than 30 Master and PhD students, received about 20 research grants, filed 8 international patents, and published more than 260 papers. Three representing works are as follows: one paper on fast block motion estimation, published in *IEEE Transactions on Circuits and Systems for Video Technology (TCSVT)* in 1994, has so far been SCI-cited more than 1000 times (Google-cited more than 2200 times) and currently stands at the 8th position among all papers published in this Transactions; one paper on smart padding for arbitrarily-shaped image blocks, published in *IEEE TCSVT* in 2001, leads to a patent that has been successfully licensed to companies; and one paper on directional discrete cosine transform (DDCT), published in *IEEE TCSVT* in 2008, receives the 2011 IEEE CSVT Transactions Best Paper Award. He also received the best paper award at ChinaCom three times (2009 Xian, 2010 Beijing, and 2012 Kunming).

He served as an Associate Editor for *IEEE TCSVT* for 8 years and received the Best Associate Editor Award in 2011. He was General Co-Chair of VCIP-2016 and PCM-2017. He received a 2nd Class Natural Science Award (the first recipient) from Chinese Ministry of Education in 2014 and was elected as an IEEE Fellow in 2016 for contributions to image and video coding.